THE GERONTOLOGICAL SOCIETY OF AMERICA®

Journals of Gerontology: Biological Sciences
cite as: *J Gerontol A Biol Sci Med Sci*, 2018, Vol. 73, No. 10, 1330–1338
doi:10.1093/gerona/gly059
Advance Access publication 21 May 2018

OXFORD

Original Article

The Protective Effect of Melatonin Against Age-Associated, Sarcopenia-Dependent Tubular Aggregate Formation, Lactate Depletion, and Mitochondrial Changes

Ramy K. A. Sayed, PhD,[1,2] Marisol Fernández-Ortiz, BSc,[1,3] María E. Diaz-Casado, PhD,[1,3] Iryna Rusanova, PhD,[1,3,4] Ibtissem Rahim, PhD,[1,5] Germaine Escames, PhD,[1,3,4] Luis C. López, PhD,[1,3,4] Doaa M. Mokhtar, PhD,[6] and Darío Acuña-Castroviejo, MD, PhD[1,3,4]

[1]Instituto de Biotecnología, Centro de Investigación Biomédica, Parque Tecnológico de Ciencias de la Salud, Universidad de Granada, Spain. [2]Department of Anatomy and Embryology, Faculty of Veterinary Medicine, Sohag University, Egypt. [3]Departamento de Fisiología, Facultad de Medicina, Universidad de Granada, Spain. [4]CIBER de Fragilidad y Envejecimiento, Ibs. Granada, Unidad de Gestión Clínica de Laboratorios Clínicos, Complejo Hospitalario de Granada, Spain. [5]Laboratory of Cellular and Molecular Biology, Faculty of Science Biologiques, University of Science and Technology Houari Boumedienne (USTHB), Algeria. [6]Department of Anatomy and Histology, Faculty of Veterinary Medicine, Assiut University, Egypt.

Address correspondence to: Darío Acuña-Castroviejo, MD, PhD, Centro de Investigación Biomédica, Parque Tecnológico de Ciencias de la Salud, Avda. del Conocimiento s/n, 18016 Granada, Spain. E-mail: dacuna@ugr.es

Received: November 9, 2017; Editorial Decision Date: March 8, 2018

Decision Editor: Rafael de Cabo, PhD

Abstract

To gain insight into the mechanism of sarcopenia and the protective effect of melatonin, the gastrocnemius muscles of young (3–4 months), early-aged (12 months), and old-aged (24 months) wild-type C57BL/6J female mice were examined by magnetic resonance and microscopy. Locomotor activity, lactate production, and nuclear apoptosis were also assessed. The results support the early onset of sarcopenia at 12 months of age, with reduction of muscle fiber number, muscle weight/body weight ratio, lactate, and locomotor activity. Lipid droplet infiltration and autophagosomes were also detected. These changes driven little effects on the early-aged muscle, but they got worse in old-aged animals by the progressive damage of the muscle. Old-aged muscle showed a reduction of the mitochondrial number, a destruction of the mitochondrial cristae, and swelling. Tubular aggregates and nucleic acid fragmentation were the most striking findings in old-aged muscle, reflecting a broad damage with loss of autophagy efficacy. Oral melatonin administration conserved the normal muscular architecture, weight, muscle fiber number, and activity in the old age; it stimulated lactate production, prevented mitochondrial damage and tubular aggregates, and reduced the percentage of apoptotic nuclei in aged muscles. Altogether, gastrocnemius muscle showed age-mediated signs of sarcopenia that were reduced by melatonin treatment.

Keywords: Aging, Autophagosome, Melatonin, Gastrocnemius, Sarcopenia

Aging courses with progressive loss of mass and contractile force of the skeletal muscle, causing a decline in muscle function and resulting in a major effect on life's quality (1). Accumulation of genetic damage and mutations in aged mitochondrial DNA (2) underlie these changes.

Sarcopenia describes the reduction of muscle strength and mass that takes place with healthy aging. This phenomenon was widely observed during mammalian aging (3–6), and it can lead to increased morbidity and mortality (7,8). Although the etiology of sarcopenia is not clearly defined, a number of mechanisms involved in this phenomenon have been suggested; these include denervation of skeletal muscle fiber; increased levels of nuclear apoptosis; enhanced oxidative stress, altered hormonal environment, and increased inflammation (9–11). Progressive losses of motor neurons and terminal axons

are proposed to be the main contributor in the aging muscle impairment (12). Terminal axon loss has been reported in muscles of both humans (13) and rats (14).

Melatonin, or *N*-acetyl-5-methoxytryptamine (aMT), is a hormone that, besides in the pineal gland (15), is widely produced by most of the organs and tissues of the body, including the skeletal muscle (16). In addition to its involvement in the control of various physiological functions of the body, melatonin exhibits powerful antioxidative and anti-inflammatory effects (17–19). The main intracellular target of melatonin is the mitochondria, where it boosts their bioenergetic properties, reduces the formation of free radicals, and enhances the production of ATP in both normal and pathological conditions (20–24). Melatonin administration also maintains the integrity of muscle mitochondrial function during aging (25,26) and improves the redox status in resistance-training athletes (27,28).

We previously observed morphological markers of sarcopenia in the gastrocnemius muscle (GM) of mice at the early stage of aging. Among these, the presence of centrally located nucleus in muscle fibers, increase of skeletal muscle fiber area, reduction of type II muscle area percentage, and increase of number and cross-sectional area (CSA) of the intermyofibrillar (IMF) mitochondria were reported in 12-month-old mice (29).

Thus, to have a better understanding of the mechanisms underlying the progress of sarcopenia during aging, as well as the protective effect of melatonin, we evaluated here the age-mediated changes in the muscular mass, locomotor activity, lactate production, and ultrastructure of the GM of the mice from 3 to 24 months of age with and without melatonin treatment.

Materials and Methods

Animals

Wild-type C57BL/6J female mice were purchased from Harlan Laboratories (Barcelona, Spain), maintained in the Granada University's facility with controlled temperature (22°C ± 1°C) and light:dark cycle (12-hour light/12-hour dark cycle, lights on at 08:00 am) and with a standard rodent chow and tap water ad libitum. All experiments were performed in accordance with the University of Granada's Ethical Committee (CEEA 462-2013); the directive 2010/63/EU of the Spanish Protection Guide for Animal Experimentation (R.D. 53/2013); and the European Convention for the Protection of Vertebrate Animals used for Experimental and Other Scientific Purposes (CETS # 123). The animals were divided into the following five groups (n = 10 animals per group): (a) mature young (Y, 3–4 months), (b) early-aged (EA, 12 months), (c) early-aged with melatonin (EA + aMT), (d) old-aged (OA, 24 months), and (e) old-aged with melatonin (OA + aMT) mice. The rodent chow contained melatonin at a concentration that allowed a daily intake of 10 mg/kg bw/mouse for 2 months before sacrifice. Although some reports showed that C57/BL6 mice could be considered melatonin-deficient mice (30,31), we and others showed that they produce melatonin from pineal and extrapineal tissues. Besides, C57/BL6 mice have been used in other experiments and they respond well to melatonin therapy (32,33). So, this mice strain is suitable for the purpose of this study.

Magnetic Resonance Imaging and In Vivo Lactate Spectroscopy

The magnetic resonance experiments were conducted with a small-animal horizontal 7 Tesla USR Bruker BioSpec TM 70/20 USR magnet (Bruker Española, S.A., Madrid, Spain). Before imaging, mice were anesthetized with isoflurane (1.5% in air), and the breathing rate was monitored using an air balloon placed on the top of the lungs (SA Instruments, Inc., New York, NY). The respiration rates between mice were similar for every experiment. For GM imaging, axial T2-weighted images were acquired using rapid acquisition with relaxation enhancement (T2 Turbo RARE) sequence (TR/TE_{eff} = 950/24 ms, matrix size = 256 × 256, rare factor = 8, field of view = 40 × 40 mm^2, 12 slices, slice thickness = 1 mm, averages = 1).

For in vivo lactate spectroscopy, multislice spin-echo and T2-weighted anatomical images were obtained. A single voxel with dimensions of 3 × 3 × 3 mm^3 was placed within the muscle, and a spectrum was acquired using a PRESS sequence with the following parameters: repetition time, the time between each initial excitation of the magnetization (TR) = 2,500 ms, echo time, the time the magnetization is in the transverse plane after an excitation before signal readout (TE) = 35 ms, number of averages = 256.

Assessment of the Locomotor Activity

The locomotor activity behavior (total distance, resting time, and mean speed) of the experimental animals was studied by the means of an open-field test. It consisted of a square area in a ground space of 25 × 25 × 25 cm, with opaque walls, so that the animals could not see the room. Each mouse was placed in the center of the square arena at 9 pm under red light exposure, and its movement was monitored through the SMART video-tracking system (Harvard Apparatus Panlab, S.L., v.3.0.03, Barcelona, Spain). Animals were placed for 30 minutes after an adaption period of 30 minutes. Distance moved (centimeter), resting time (%), and mean speed (centimeter per second) of each mouse were quantified. Digital images representing the maps of the locomotor activity were acquired.

The speed and fatigue (running distance and time of exhaustion) were tested by using a treadmill system (Panlab LE 8710 Treadmill control, Barcelona, Spain). Because behavioral variability between individuals of the same group is high, the environmental variables must be constant throughout the study (light, humidity, background, and noise) as well as time, age, and the sex of the animal. Before experiments with treadmill, the animals were prior adapted for 3–5 days at a constant rate of 9 cm/s for 20 minutes to become familiar with the apparatus. At the day of experiment, the body weight of the animals was measured, and the apparatus speed was initially adjusted at 9 cm/s for 5 minutes and then the speed was increased 2 cm/s every minute until the mouse reached exhaustion. (The point of exhaustion was considered when the mouse stopped running on the treadmill for more than 10–20 seconds.) The animals then were rested for 1 week before sacrificing.

Calculation of Frailty Index

A clinical frailty index (FI) has been proposed and validated in animals including mice and primates that correlates with the human index (34–38). Accordingly, and using the clinical criteria used in humans (39,40), we calculated the FI index from the variables weight = muscle weight/body weight ratio; endurance = exhaustion time and resting time; slowness = mean speed, and physical activity = total distance and traveled distance. Mean ± *SD* values for each parameter were recalculated (data in Supplementary Figure 3 are expressed as the mean ± *SEM*) as shown in Supplementary Table 1. The data corresponding to the young group (Y group) were used as reference values, and frailty index was calculated as follows: the data that differed by ±1 *SD* with respect to the reference group were given a frailty index of 0.25; those that differed by ±2 *SD* received a frailty index of 0.5; values over ±3 *SD* were given a value of 0.75, and those above ±3

SD received the maximal value of 1. The values for each group were summed and divided by the number of items analyzed, given the final FI score. Because melatonin treatment improved the scores in the variables used, the individual frailty indexes calculated for these groups were given a negative value when they were above the value of the reference group (Y group) and a positive value when they were below the reference. So, increasing FI means a deterioration of the animals with age, and decreasing (negative) FI means an improvement of the physical condition of the animals, compared with Y group.

Tissue Preparation for Histological Procedures

Mice were weighted and anaesthetized by intraperitoneal injection of equithesin (1 mL/kg) and transcardially perfused with warm saline followed by a solution of freshly prepared trump's fixative (3.7% formaldehyde plus 1% glutaraldehyde in saline buffer). The GM was removed at its origin and insertion, and excess of connective tissue was dissected. The muscle was weighted and fixed in the resting length in the trump's fixative; the right muscle was divided into two halves at the mid-belly and immersed in Bouin's solution for histological examination, and small pieces from the left GM were processed for transmission electron microscopy analysis.

Proper fixed cross and longitudinal samples from the studied GM were extensively washed in ethanol 70% (3 × 24 hours) to remove fixative; then, the specimens were dehydrated in ascending graded concentrations of ethanol, cleared in xylene, and embedded in paraffin wax. Sections of 4 µm thick were cut with an SLEE Mainz Cut 5062 microtome, dewaxed in xylene (2 × 30 minutes), rehydrated in a descending series of ethanol (100%, 95%, 80%, and 70%), and washed with distilled water. The sections were stained with hematoxylin and eosin stain for general histological examination (41) and with Van Gieson stain (42) and Crossmon's trichrome stain (43) for differentiation of connective tissue and muscle fibers. After staining, the sections were dehydrated again in an ascending series of ethanol (70%, 95%, and 100%), cleared in xylene (2 × 10 minutes), and mounted with DPX. The sections were examined, and digital images were acquired using a Carl Zeiss Primo Star Optic microscope and a Magnifier AxioCamICc3 digital camera (BioSciences, Jena, Germany).

Fluorescent Detection of Apoptotic Nuclei

For demonstration of apoptotic nuclei, 4-µm-thick paraffin sections were dewaxed in xylene, rehydrated in a descending series of ethanol, and washed with distilled water. The sections were air-dried and rinsed in phosphate-buffered saline 1× (2 × 5 minutes) and stained with 33258 Hoechst dye (H6024, Sigma–Aldrich, Madrid, Spain) for 1 hour. Following staining, the sections were washed in phosphate-buffered saline 1× (5 × 5 minutes), air-dried, mounted, examined with LEICA DM5500B fluorescent microscope, and detected the apoptotic nuclei ratio. Hoechst dye is a fluorescent dye that penetrates the nucleus of a cell and binds to DNA. When viewed under a light at near 350-nm wavelength, the dye emits blue fluorescent light that effectively makes the DNA in the nucleus visible (44).

Transmission Electron Microscopy

Fresh small pieces of GM were fixed in a 2.5% glutaraldehyde in 0.1 M cacodylate buffer (pH 7.4) and then postfixed in the same buffer containing 1% osmium tetraoxide plus 1% potassium ferrocyanide for 1 hour. The samples were then passed on 0.15% tannic acid for just 50 seconds, incubated in 1% uranyl acetate for 1.5 hour with shaking, dehydrated in ethanol, and embedded in resin. Ultrathin sections (65 nm thick) were cut by a Reichert-Jung Ultracut E ultramicrotome, double stained with uranyl acetate and lead citrate (45), and examined on a Carl Zeiss Leo 906E electron microscope.

Morphometrical Analyses

Morphometrical measurements of the CSA, perimeter, and Feret's diameter of the individual skeletal muscle fibers were obtained from the images of Grossmon's trichrome-stained paraffin cross sections acquired by optic microscope at a ×40 objective magnification, whereas the total number of skeletal muscle fibers was obtained from the images of Van Gieson-stained paraffin cross sections taken at a ×10 magnification. Analysis of IMF mitochondrial number was applied on images of transmission electron microscopy on area measured 7,790 nm width and 5,929 nm height, and analysis of subsarcolemmal (SS) mitochondrial number was detected on area measured 5,249 nm width and 3,995 nm height. All these measurements were performed using Image J processing software.

Statistical Analyses

All statistical analyses were performed using Prism 6 software package (GraphPad, La Jolla, CA), and the data presented as mean ± *SEM* of $n = 5$ animals per group. One-way analysis of variance was used for statistical comparisons, and differences were considered significant when $p < .05$. For in vivo lactate spectroscopy, intraclass correlation estimates and their 95% confidence intervals were calculated using SPSS statistical package version 24.0 (SPSS Inc., Chicago, IL). Before analysis of in vivo lactate spectroscopy, a reliability study to evaluate its test–retest reliability was performed. The study was carried out in 10 mice, and measurements were repeated three times for each mouse. These data were analyzed using a single-measurement, absolute-agreement, two-way mixed-effects model, reporting an intraclass correlation of .88 with 95% confident interval and concluding that the test–retest reliability for this method is good.

Results

Magnetic Resonance Examination and In Vivo Lactate Spectroscopy

Magnetic resonance imaging on wild-type mice of different ages revealed a clear age-related decline in the CSA of the leg region (young mice [Y], 3.7 ± 0.2 mm; early-aged mice [EA], 3.1 ± 0.3 mm; and old-aged mice [OA], 2.5 ± 0.2 mm muscular diameter, $p < .05$). Melatonin supplementation diminishes the loss of muscle area in the early-aged muscle (EA + aMT, 3.3 ± 0.1 mm), but not in the old-aged muscles (OA + aMT, 2.5 ± 0.4 mm; Supplementary Figure 1).

In vivo lactate spectroscopy, the findings on the GM of the young (Y), early-aged (EA), and old-aged animals (OA) illustrated an age-mediated reduction in the production of lactate, reflecting that anaerobic respiration activity decreases with aging. This reduction was countered by melatonin that stimulated lactate production (Supplementary Figure 2).

Behavioral Analysis

Recordings of the locomotor activities are depicted in Supplementary Figure 3. In video-tracking open-field test, young animals (Y) and early-aged animals (EA) revealed no changes in the total distance, resting time, and mean speed. By contrast, old-aged (OA) animals moved to a shorter distance, with longer resting time, and lower mean speed (Supplementary Figure 3A). Melatonin supplementation increased the total distance moved and the mean speed, with reduction of the resting time in both early- and old-aged animals). These changes are

clarified in the acquired maps of the movement activity (Supplementary Figure 3B). In the treadmill test, early-aged animals traveled to a longer distance and resisted the exhaustion for a longer time than young animals. At the old age, the animals moved to a shorter distance and became exhausted faster. These latter changes were reversed, and the activity was enhanced by melatonin (Supplementary Figure 3C).

Anthropometric Analysis of Body Weight and Muscle Weight With Aging

Body weight and GM weight increased with age (Supplementary Figure 4). Body weights (Supplementary Figure 4A) of young, early-aged, and old-aged animals were 21.6 ± 0.47, 28.88 ± 0.41, and 31.82 ± 0.46 g, respectively ($p < .05$), whereas muscle weights (Supplementary Figure 4B) were 139.5 ± 1.45, 148.1 ± 3.03, and 164.6 ± 2.15 mg, respectively ($p < .05$). The ratio of the muscle weight to body weight (Supplementary Figure 4C), however, decreased significantly with age, from 0.65% in young animals to 0.55% in early-aged animals and 0.52% in old-aged animals ($p < .05$).

Melatonin supplementation increased the body weight of the early- and old-aged animals (30.20 ± 0.47 and 33.3 ± 0.33 g, respectively, $p < .05$), with induction of muscle weight increase in early-aged mice (168.8 ± 0.67 mg, $p < .05$) and old-aged mice (180.1 ± 0.38 mg, $p < .05$). In addition, melatonin treatment induced the ratio of muscle weight to body weight in both early- and old-aged muscles (0.58% and 0.55%, respectively, $p < .05$).

FI Index

The frailty index calculated for each group of age compared with the young (Y) group is shown in Supplementary Figure 5. Age enhances the FI index, which was significantly elevated in OA animals compared with young animals (0.58, $p < .05$). Treatment with melatonin recovered the age-dependent physical impairments in both EA and OA groups of mice.

Light Microscopical Changes of the Gastrocnemius Muscle in Young Mice

Muscles of the young wild-type mice (Y) showed a normal structure of muscle fibers that arranged in bundles, separated by a narrow perimysium (P) and endomysium (e), supporting blood capillaries (BC) and nerve fibers (Ne; Supplementary Figure 6A–C). Skeletal muscle fibers of both early-aged (EA; Supplementary Figure 6D–F) and old-aged (OA; Supplementary Figure 6G–I) animals showed age-related changes including hypertrophy of the muscle fibers, increasing the endomysium and perimysium spaces with abundant collagenous tissue (Col) infiltration, as well as a centrally located nucleus in 24% of the fibers of the early-aged animals, which increased to about 38% in the old-aged animals. In old-aged mice, large irregular damaged areas were observed within the muscle fibers.

Melatonin administration revealed a protective effect on the muscle fibers of both early-aged mice (Supplementary Figure 6J–L) and old-aged mice (Supplementary Figure 6M–O). The fibers conserved their normal architecture with the nucleus located peripherally, narrow interstitial spaces, and less collagenous tissue accumulations. Moreover, the internally damaged areas of muscle fibers were missed in the protected aged groups.

Age-Related Morphometrical Changes of Individual Muscle Fiber

Aging induced the increase of individual muscle fiber CSA (Supplementary Figure 7A) from 591.8 ± 36.50 μm² in young animals to 1,823 ± 65.61 μm² in early-aged animals and 2,037 ± 73.26 μm² in old-aged animals ($p < .05$). This increase of CSA was associated with increase of muscle fiber's perimeter (Supplementary Figure 7B) and Feret's diameter (Supplementary Figure 7C) from 100.3 ± 3.48 and 35.39 ± 1.66 μm, respectively, in young animals to 192.8 ± 6.42 and 68.23 ± 1.92 μm in early-aged animals and 200 ± 4.01 and 74.06 ± 2.03 μm in old-aged muscles ($p < .05$). Aging, however, reduced the number of muscle fibers (Supplementary Figure 7D) from 5,848 ± 183 in young animals to 5,178 ± 52 in early-aged animals and 3,881 ± 90 in old-aged animals ($p < .05$).

Melatonin administration countered the increase of muscle fiber CSA in early-aged animals (1,683 ± 64.66 μm²) and old-aged animals (1,436 ± 95.94 μm², $p < .05$), with reduction of muscle fiber's perimeter and Feret's diameter in early-aged animals (172 ± 1.77 and 60.07 ± 0.85 μm, respectively, $p < .05$) and in old-aged animals (161.6 ± 4.89 and 59.70 ± 2.42 μm, respectively, $p < .05$). Interestingly, melatonin treatment slightly increased the muscle fiber number in the early-aged muscle (5,620 ± 1,742) and highly stimulated muscle fibers number in the old-aged muscle (5,045 ± 181, $p < .05$).

Age-Induced Ultrastructural Changes in Gastrocnemius Muscle

Electron microscopy examination of the young GM demonstrated a normal architecture with the organization of muscle fibers into bundles and the nucleus (N) of the fibers located peripherally (Figure 1A). The myofibril (Mf) composition of the individual fibers, consisted of both thick myosin and thin actin filaments, is shown. Moreover, the IMF distributions of the sarcoplasmic reticulum (SR) and mitochondria (M) can be also observed (Figure 1B). Furthermore, the longitudinal striations of the skeletal fibers were clearly depicted in the Mf of the young animals, illustrating the arrangements of the myofilaments in the anisotropic (A-band) and isotropic bands (I-band), as well as associated IMF components of mitochondria (M) and SR (Figure 1C).

In the early-aged animals, some skeletal muscle fibers showed a normal structure of the Mf with the nuclei (N) presented peripherally (Figure 2A). However, some fibers demonstrated centrally located nuclei (Figure 2B). Among other changes observed in this stage, it can be noted an increase of lipid droplet (L) infiltration lodged between the mitochondria (M; Figure 2C) and near the nucleus (N; Figure 2D), with appearance of few peripherally positioned multivesicular bodies

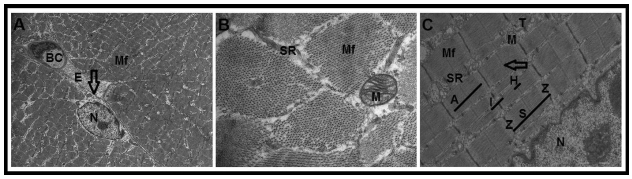

Figure 1. Ultrastructure of the gastrocnemius muscle. (**A**) Electron micrograph of a cross section of the gastrocnemius muscle of the young animals, showing the individual muscle fiber (arrow) constituted of myofibrils (Mf) and separated from each other by endomysium (E), which supports network of blood capillaries (BC). The nucleus (N) has its normal position peripherally. (**B**) Electron micrograph of higher magnification illustrating the arrangement of the actin and myosin myofilaments in the Mf, with the intermyofibrillar distribution of the sarcoplasmic reticulum (SR) and mitochondria (M). (**C**) Electron micrograph of a longitudinal section of the muscle fibers from the young animals clarifying the cross striations seen by light microscopy. Mf, myofibrils; Z, Z-line; S, sarcomeres; A, A-band; I, I-band; H, H-zone; arrow, M-line; M, Mitochondria; T, transverse tubules; and SR, intermyofibrillar distribution of the sarcoplasmic reticulum. (**A**) Scale bar = 5 μm; (**B**) scale bar = 1 μm; (**C**) scale bar = 2 μm.

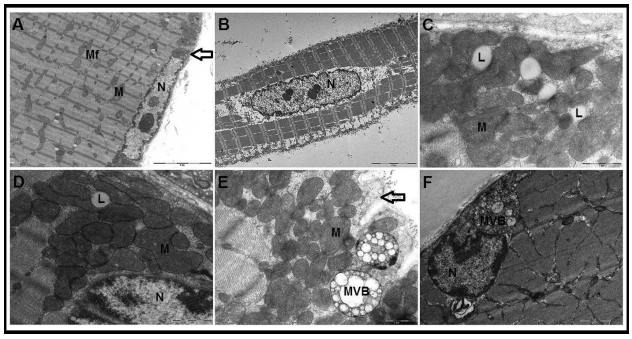

Figure 2. Early ultrastructural changes of the gastrocnemius muscle with aging. (**A**) Electron micrograph of the skeletal muscle of the early-aged animals revealing the organization of the myofibrils (Mf) in the muscle fibers and distribution of the mitochondria (M) in between. The nucleus (N) in some fibers is found peripherally, just beneath the sarcolemma (arrow). (**B**) Some muscle fibers at the early age demonstrate a centrally located nucleus (N). (**C** and **D**) Electron micrographs depicting increase of the lipid droplet (L) infiltrations between the mitochondria (M), and close to the nucleus (N). (**E** and **F**) Muscle fibers of the early-aged animals illustrating the formation of multivesicular bodies (MVB) described as autophagosomes. These bodies are observed peripherally, under the sarcolemma (arrow), close to the mitochondria (M) and nucleus (N). (**A** and **B**) Scale bar = 5 μm; (**C**–**E**) scale bar = 1 μm; (**F**) scale bar = 2 μm.

described as autophagosomes, which were closed to the mitochondria, nucleus, and also under the sarcolemma (Figure 2E and F).

In the old-aged muscle, some fibers were found normally with a few IMF mitochondria showing cristae damage (Figure 3A). In addition, some fibers illustrated sarcomeres disorganization (Figure 3B); excessive collagen matrix (Figure 3C); severely damaged mitochondria with a destructed cristae (Figure 3C and F); and centrally located nucleus with accumulation of glycogen droplets (G; Figure 3D). The detected autophagosomes in the early-aged muscle were much more numerous in the old-aged mice on both IMF and SS positions (Figures 3E–H). Concentric arrangements of the smooth endoplasmic reticulum were also peripherally apparent (Figure 3I).

Interestingly, electron microscopy illustrated the irregular damaged areas that were observed in the old-aged muscles by light microscopy. These abnormalities were detected beneath the sarcolemma (Figure 4A), in the center of the muscle fibers (Figure 4A and B), and also close to the nucleus (Figure 4C), which are centrally located. By higher magnification, these areas showed presence of differently oriented membranous tubular aggregates (TAs; Figure 4B), with some of these tubules with a central core (Figure 4I). Among the structures sharing the formation of these aggregates, were SR, mitochondria, and smooth endoplasmic reticulum (Figure 4D and E). Connections between the mitochondria and SR at the peripheral regions of TAs were identified (Figure 4F). Some damaged areas revealed dissociation of the TAs (Figure 4G) and formation of the multivesicular bodies (Figure 4H).

Electron microscopy examination of the protective effects of melatonin treatment was clearly apparent in both early-aged (Figure 5A–C) and old-aged (Figure 5D–F) muscles. Melatonin kept normal or less damaged muscle fibers architecture with aging. The fibers were observed with normally positioned nuclei, Mf organization, sarcoplasmic arrangement, and normally compacted mitochondria, with few damaged cristae. The formation of the TAs was not observed under melatonin treatment.

Morphometrical analysis shown in Supplementary Figure 8 revealed no significant changes in the number of IMF and SS

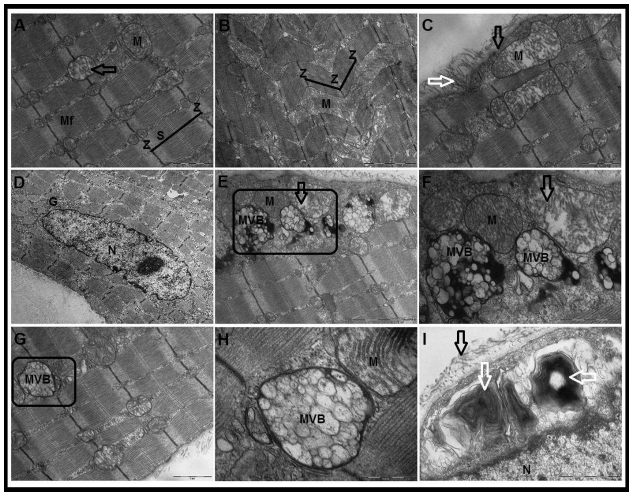

Figure 3. Ultrastructural changes of the gastrocnemius muscle at the late stage of aging. (**A**) Electron micrograph of the muscle fibers of the old-aged animals showing the myofibrils (Mf), sarcomere (S), Z-line (Z), and mitochondria (M). Some intermyofibrillar mitochondria are observed vacuolated with destructed cristae (arrow). (**B**) Muscle fiber illustrating disorganization of the sarcomere (S) and Z-lines (Z) with enlarged mitochondria (M). (**C**) Severe damaged and enlarged subsarcolemmal mitochondria (M) are demonstrated under the sarcolemma (black arrow) with excessive collagen matrix (white arrow). (**D**) Muscle fibers with centrally located nucleus (N), which are surrounded by excessive glycogen droplets (G). (**E** and **F**) Muscle fibers demonstrating the presence of peripherally intact mitochondria (M) with compacted cristae, damaged mitochondria with destructed folds (arrow), and multivesicular bodies (MVB). (**G** and **H**) The appearance of intermyofibrillar multivesicular bodies (MVB) close to the mitochondria (M). (**I**) Concentric arrangement of the smooth endoplasmic reticulum (white arrow) peripherally between the nucleus (N) and the sarcolemma (black arrow). (**A**, **C**, **F**, **G**, and **I**) Scale bar = 1 μm; (**B**, **D**, and **E**) scale bar = 2 μm; (**H**) scale bar = 500 nm.

mitochondria in the early-aged muscles (25 ± 1.2 and 23 ± 1.25, respectively, in young animals vs. 26 ± 1 and 27 ± 1.3, respectively, in early-aged animals). In old-aged muscle, there was a significant decline in the number of IMF mitochondria (16 ± 1.3, $p < .05$) and SS mitochondria (14 ± 1.2, $p < .05$). Melatonin treatment reported no changes in the early-aged animals (26 ± 1.17 and 27 ± 1.30 in IMF and SS mitochondria, respectively), and maintained higher IMF (21 ± 1, $p < .05$) and SS (20 ± 1.23, $p < .05$) mitochondrial number in the old-aged mice.

Hoechst Analysis of the Apoptotic Nuclei

The nuclei of the skeletal muscle of the young animals (Y) as shown by Hoechst fluorescent detection revealed normal appearance (Supplementary Figure 9A). With aging, some nuclei showed signs of chromatin condensation and fragmentation of the nucleic acid, which were clearer in the old-aged muscles (Supplementary Figure 9D) than those of the early-aged muscles (Supplementary Figure 9B). Moreover, aging induced a progression in the percentage of the apoptotic nuclei that was reduced by melatonin administration (Supplementary Figure 9C and E).

Discussion

Aging is associated with a progressive and irreversible decline in the functions of the body as a result of biochemical and morphological changes (46). Among these alterations, skeletal muscle is one of the

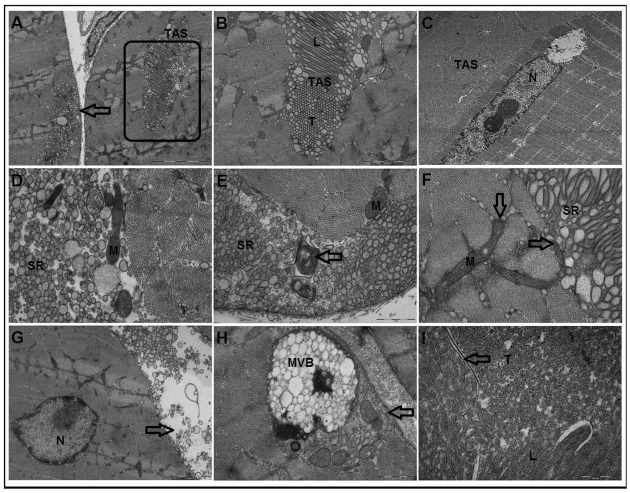

Figure 4. Tubular aggregates (TAs) formation in the old-aged gastrocnemius muscle. (**A**) Electron micrograph of the muscle fibers of the old-aged animals showing the formation of TAs within the fibers and peripherally under the sarcolemma (arrow). (**B**) Higher magnification of the TAs illustrating longitudinal (L) and transverse (T) orientations. (**C**) Formation of the TAs close to the nucleus (N), which demonstrated centrally position. (**D** and **E**) Structures share in the formation of TAs including sarcoplasmic reticulum (SR), mitochondria (M), and smooth endoplasmic reticulum (arrow). (**F**) Electron micrograph clarifying the connections (arrow) between the mitochondria (M) and sarcoplasmic reticulum (SR) at the peripheral regions of the TAs. (**G**) Dissociation of the tubular aggregates (arrow). Note the presence of centrally located nucleus (N). (**H**) Formation of the multivesicular bodies (MVB) under the sarcolemma (arrow). (**I**) Electron micrograph of higher magnification of the TAs depicting the longitudinal (L) and transverse (T) orientations, with some tubules having a central core (arrow). (**A** and **C**) Scale bar = 5 μm; (**B** and **G**) scale bar = 2 μm; (**D**, **E**, **F**, and **H**) scale bar = 1 μm; (**I**) scale bar = 500 nm.

most strikingly affected tissues with age, resulting in loss of muscular mass and strength, a phenomenon identified as sarcopenia, which is accompanied by morphological changes that influence muscle function (5–7). In this regard, about 40% of the human muscle is wasted from 20 to 80 years of age, associated with muscle strength decline (47). The etiology of the sarcopenia is still unclear, but several mechanisms depending on muscle atrophy and fiber loss have been proposed (9,48). Our results confirmed the muscular atrophy with age, with a clear age-related reduction in the CSA of the leg region identified by magnetic resonance imaging (29).

Oxidative muscle fibers (type II) are metabolically suited for lactate oxidation, and they have a greater capacity for sarcolemmal lactate transport than do glycolytic muscle fibers (type I) (49). Thus, lactate production reflects the balance between aerobic versus anaerobic metabolism, and its levels in the muscle may yield important information regarding the changes in muscle fiber's composition and metabolism during aging. Moreover, lactate crosses membranes in skeletal muscle through several monocarboxylate transporters (MCT1-4); specifically, MTC1 is correlated with the uptake of lactate from the circulation and the oxidative capacity of skeletal muscle. Training enhances MCT1 and lactate transport to the muscle, whereas aged muscle had a reduction in MCTs and, thus, diminished the lactate levels and increases fatigue in skeletal muscle (50). By in vivo spectroscopy, we detected a reduction in the ratio of lactate absorbance in the mouse GM with age, which agree with the marked loss of the locomotor activity and fatigue with age here reported. However, other study (51) reported an increase in plasma lactate

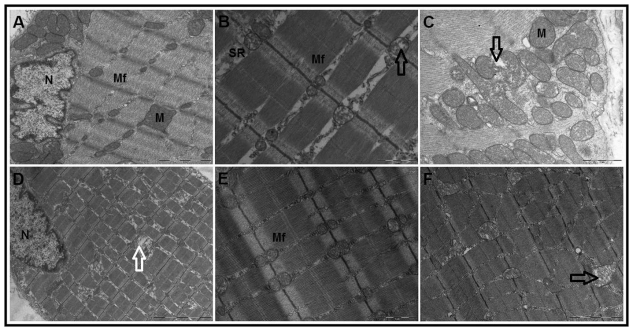

Figure 5. The protective effect of melatonin against the age-associated damage of the skeletal muscle. (**A–C**) and (**D–F**) Electron micrographs of the muscle fibers of the protective early-aged and old-aged animals, respectively, showing the protective effect of melatonin on conserving the normal ultrastructure of the myofibrils (Mf) with the nuclei (N) peripherally located, and the intermyofibrillar distribution of the mitochondria (M) and sarcoplasmic reticulum (SR). Few mitochondria illustrated damaged cristae (arrow), whereas others are normal and compacted. The formation of the tubular aggregates was not observed. (**A** and **F**) Scale bar = 2 μm; (**B**, **C**, and **E**) scale bar = 1 μm; (**D**) scale bar = 5 μm.

levels in wild-type and dwarf mice from 3 to 12 months, followed by its reduction at 18 months of age.

Maintenance of skeletal muscle mass and quality has a substantial role in prevention of age-related decline in metabolic function and physical frailty (52). The association between low muscle mass and functional decline seems to be a function of underlying muscle strength (53), which was demonstrated as a marker of muscle quality that is more important in estimating mortality risk (54). The qualitative change observed in skeletal muscle appears to be related to muscle structure and composition (55).

To gain insight on how changes in locomotor activity, skeletal muscle mass, and lactate reflect the progress of sarcopenia, light and electron microscopical analyses were performed. In mice of 12 months of age, that is, early-aged animals, we previously detected a loss of the muscle fibers and a compensatory increase in the average fiber's area, which was extended to both fiber types in the GM (29). We report now that 24-month-old mice had an excess of accumulated collagenous tissue in the perimysium of GM (56), a sign of fibrosis. This collagen accumulation could have two important significances in the aged muscle: (a) the consequent increase of the extracellular matrix, which reduces the lateral force transmission of the muscle (57), and (b) the increase of extracellular water in detriment of the intracellular water, which may underline the finding that the relative expansion of the former correlates with the reduced muscle performance with age (58).

The presence of centrally located nuclei described in early-aged mice (29) further increased in the muscle of old-aged mice, which might be a critical sign of fiber's degeneration and regeneration (29,59). These changes were accompanied by high percentage of apoptotic nuclei, which was suggested to participate in the onset and progress of sarcopenia (9,10).

Numerous studies correlated aging with mitochondrial impairment (60). By electron microscopy, our data confirmed the increased lipid droplets, mitochondrial aggregates, and mitochondrial structure damage, which appears swollen with destructed cristae and matrix vacuolization. These findings are indicators of cell senescence (61) and support the loss of the normal mitochondrial function with age elsewhere reported (25,26). These studies revealed an age-dependent mitochondrial oxidative damage in cardiac and

diaphragmatic muscles of mice, accompanied by a reduction in both the electron transport chain activity and ATP production.

Damaged mitochondria are under selective sequestration and fragmentation by autophagy/mitophagy, although abnormal mitophagy due to increased mitochondrial fragmentation initiates apoptotic processes and cell death. Our results show the formation of autophagosomes as multivesicular bodies, reflecting the induction of the autophagic processes in the GM at early and old stages of age. Autophagy displays cellular component degradation visible within the intact dying cell in autophagic vacuoles, with morphological features of vacuolization and degradation of cytoplasmic contents, and chromatin condensation; these autophagic cells can also be phagocytosed. The autophagic/mitophagic capacity declines during aging, causing accumulation of reactive oxygen species produced by dysfunctional mitochondria and resulting in activation of the NLRP3 inflammasome and induction of low-grade inflammation in several tissues accelerating the aging process (19,62). Moreover, the extensively damaged mitochondria by reactive oxygen species in aged skeletal muscle causes cytoskeleton reorganization, DNA damage, nuclear structure disruption, and disintegration of the cell into apoptotic bodies, leading to cell death (63).

Among the striking ultrastructural changes in the GM of the old-aged animals, the severe damage of the fibers with the aggregations of tubular-like inclusions (TAs) is noticeable. These aggregations were visible in the center of the fibers and peripherally beneath the sarcolemma. Although the exact mechanism underlying TA formation and function in skeletal muscle is still unclear, previous studies revealed that TAs arise from the components of the SR in skeletal muscle of almost all normal inbred mice strains in relation to both sex and age (64,65), and they suggested that TA results from reshaping of SR caused by misfolding and aggregation of membrane proteins (66). Another study on GM of $CK^{-/-}$ mice revealed the presence of mitochondrial enzymes in TAs, suggesting the participation of both mitochondria and SR in the formation of TAs (67). Our results confirmed the dual mitochondrial and SR origin of TAs, revealing the implication of damaged mitochondria and SR in the formation of the TAs, with connections between the mitochondria and TAs were demonstrated.

Melatonin, an indoleamine produced by both pineal and extrapineal tissues (16), exerts important antioxidant and anti-inflammatory functions (15), protecting the cell and boosting the mitochondrial bioenergetic capacity (18,20–22,68). Melatonin improves the muscle function and reduces the oxidative stress and inflammation in athletes (27,28,69) and recovers mitochondria from several injuries (19,23,24). The dose of 10 mg/kg/melatonin used here, has also proven significant anti-aging benefits in SAM mice (25,26). We previously reported that the therapeutical doses of the melatonin range from 5 mg to 50 mg/kg bw (70). In this study, and using the human equivalent dose formula, we calculated that 10 mg/kg in rats correspond to 1.62 mg/kg for an adult of 60 kg bw, which is about 97.3 mg/d. Doses 50 mg to 300 mg/d have been used in some clinical studies, showing important benefits and absence of side effects (71–73). So, a clinical trial with 50–100 mg/d melatonin in patients with sarcopenia should be suggested.

Importantly, melatonin administration prevents the age-dependent mitochondrial changes in aged mice (25,26). We then decide whether these properties of melatonin may also account for the protection against age-dependent GM alterations. Our results showed that melatonin administration conserved the muscle fiber number as well as muscular mass and activity in aged animals, with induction of lactate production. Also, melatonin reduced the interstitial spaces and collagenous tissue infiltration, as well as the percentage of apoptotic nuclei in the aged muscles, reflecting the anti-inflammatory and antioxidative properties of melatonin (16). The beneficial effects of melatonin extent to maintain the normal architecture of mitochondria, SR, and Mf. Melatonin also recovers the normal autophagy process, thus avoiding the age-mediated muscle fiber damage, mitochondrial changes, and apoptosis (68). These findings confirmed the protective effect of melatonin on prevention of mitochondrial impairment, reduction of oxidative stress, autophagic alterations, and chronic low inflammation, which may account for the reduction of sarcopenic changes in patients (74). In supporting the utility of melatonin reported here, previous data showed that pinealectomized rats had skeletal muscle mitochondrial impairment and insulin resistance due to the inhibition of CREB-PGC-1 alpha pathway, whereas melatonin treatment recovered mitochondrial function via activation of CREB-PGC-1 alpha pathway (75).

It is clear from our data that GM of C57/BL6 mice displays significantly age-mediated behavioral, ultrastructural, and functional changes that clarify the onset of the sarcopenia at the early stage of age, and its progression with age, ending with marked sarcopenia that underlies a fragile condition. Melatonin behaves as an excellent protective strategy against age-dependent sarcopenia. This may be summarized in (a) the early protective effect of melatonin against age-mediated atrophy of the muscular area of the leg with aging that supports loss of the muscle mass; (b) the conservative effect of melatonin against the age-associated reduction in the locomotor activities, muscle fibers number, and lactate production, which reflects the subsequent loss of muscular strength and function in aged mice; (c) the preservative effect of melatonin in avoidance of the centrally located nucleus and increase of collagenous tissues matrix that indicate muscular degeneration and inflammation in advanced age; (d) the protective effect of melatonin against appearance and accumulation of autophagosomes that reveal autophagic process induction as a result of damaged and dysfunctional mitochondria; and (e) the beneficial effect of melatonin against TA formation that may be indicator of muscular denervation and/or myopathy.

Supplementary Material

Supplementary data is available at *The Journals of Gerontology, Series A: Biological Sciences and Medical Sciences* online.

Funding

This study was supported in part by grants from the Egyptian Cultural Bureau in Madrid, Egyptian Ministry of Higher Education, Cultural Affairs and the Missions Sector, Egypt; from the Instituto de Salud Carlos III (RD12/0043/0005, PI13-00981, PI16-00519, CB/10/00238); and from the Consejería de Economía, Innovación, Ciencia y Empleo, Junta de Andalucía (CTS-101), Spain.

Acknowledgments

We thank Mohamed Tassi and Ana M. Santos (Universidad de Granada, Spain) for their technical support with transmission electron microscopy and also Ana Fernández-Ibáñez for her technical support with magnetic resonance experiments and lactate spectroscopy.

Conflict of Interest

None reported.

References

1. Cruz-Jentoft AJ, Baeyens JP, Bauer JM, et al.; European Working Group on Sarcopenia in Older People. Sarcopenia: European consensus on definition and diagnosis: report of the European Working Group on Sarcopenia in Older People. *Age Ageing*. 2010;39:412–423. doi:10.1093/ageing/afq034
2. Moskalev AA, Shaposhnikov MV, Plyusnina EN, et al. The role of DNA damage and repair in aging through the prism of Koch-like criteria. *Ageing Res Rev*. 2013;12:661–684. doi:10.1016/j.arr.2012.02.001
3. Roubenoff R, Castaneda C. Sarcopenia – understanding the dynamics of aging muscle. *JAMA*. 2001;286:1230–1231.
4. Hughes VA, Frontera WR, Wood M, et al. Longitudinal muscle strength changes in older adults: influence of muscle mass, physical activity, and health. *J Gerontol A Biol Sci Med Sci*. 2001;56:B209–B217.
5. Marcell TJ. Sarcopenia: causes, consequences, and preventions. *J Gerontol A Biol Sci Med Sci*. 2003;58:M911–M916.
6. Visser M, Schaap LA. Consequences of sarcopenia. *Clin Geriatr Med*. 2011;27:387–399. doi:10.1016/j.cger.2011.03.006
7. Goodpaster BH, Park SW, Harris TB, et al. The loss of skeletal muscle strength, mass, and quality in older adults: the health, aging and body composition study. *J Gerontol A Biol Sci Med Sci*. 2006;61:1059–1064.
8. Narici MV, Maffulli N. Sarcopenia: characteristics, mechanisms and functional significance. *Br Med Bull*. 2010;95:139–159. doi:10.1093/bmb/ldq008
9. Buford TW, Anton SD, Judge AR, et al. Models of accelerated sarcopenia: critical pieces for solving the puzzle of age-related muscle atrophy. *Ageing Res Rev*. 2010;9:369–383. doi:10.1016/j.arr.2010.04.004
10. Marzetti E, Calvani R, Bernabei R, Leeuwenburgh C. Apoptosis in skeletal myocytes: a potential target for interventions against sarcopenia and physical frailty – a mini-review. *Gerontology*. 2010;58:99–106. doi:10.1159/000330064
11. Johnston AP, De Lisio M, Parise G. Resistance training, sarcopenia, and the mitochondrial theory of aging. *Appl Physiol Nutr Metab*. 2008;33:191–199. doi:10.1139/H07-141
12. Doherty TJ, Vandervoort AA, Brown WF. Effects of ageing on the motor unit: a brief review. *Can J Appl Physiol*. 1993;18:331–358.
13. Doherty TJ, Vandervoort AA, Taylor AW, Brown WF. Effects of motor unit losses on strength in older men and women. *J Appl Physiol*. 1993;74:868–874. doi:10.1152/jappl.1993.74.2.868
14. Sugiura M, Kanda K. Progress of age-related changes in properties of motor units in the gastrocnemius muscle of rats. *J Neurophysiol*. 2004;92:1357–1365. doi:10.1152/jn.00947.2003
15. Reiter RJ. Melatonin: the chemical expression of darkness. *Mol Cell Endocrinol*. 1991;79:C153–C158.
16. Acuña-Castroviejo D, Escames G, Venegas C, et al. Extrapineal melatonin: sources, regulation, and potential functions. *Cell Mol Life Sci*. 2014;71:2997–3025. doi:10.1007/s00018-014-1579-2
17. Reiter RJ, Mayo JC, Tan DX, Sainz RM, Alatorre-Jimenez M, Qin L. Melatonin as an antioxidant: under promises but over delivers. *J Pineal Res*. 2016;61:253–278. doi:10.1111/jpi.12360
18. García JA, Volt H, Venegas C, et al. Disruption of the NF-κB/NLRP3 connection by melatonin requires retinoid-related orphan receptor-α and blocks the septic response in mice. *FASEB J*. 2015;29:3863–3875. doi:10.1096/fj.15-273656
19. Volt H, García JA, Doerrier C, et al. Same molecule but different expression: aging and sepsis trigger NLRP3 inflammasome activation, a target of melatonin. *J Pineal Res*. 2016;60:193–205. doi:10.1111/jpi.12303
20. Martín M, Macías M, Escames G, León J, Acuña-Castroviejo D. Melatonin but not vitamins C and E maintains glutathione homeostasis in t-butyl hydroperoxide-induced mitochondrial oxidative stress. *FASEB J*. 2000;14:1677–1679. doi:10.1096/fj.99-0865fje
21. Martín M, Macías M, León J, Escames G, Khaldy H, Acuña-Castroviejo D. Melatonin increases the activity of the oxidative phosphorylation enzymes and the production of ATP in rat brain and liver mitochondria. *Int J Biochem Cell Biol*. 2002;34:348–357.
22. López A, García JA, Escames G, et al. Melatonin protects the mitochondria from oxidative damage reducing oxygen consumption, membrane potential, and superoxide anion production. *J Pineal Res*. 2009;46:188–198. doi:10.1111/j.1600-079X.2008.00647.x
23. Escames G, León J, Macías M, Khaldy H, Acuña-Castroviejo D. Melatonin counteracts lipopolysaccharide-induced expression and activity of mitochondrial nitric oxide synthase in rats. *FASEB J*. 2003;17:932–934. doi:10.1096/fj.02-0692fje
24. Escames G, López LC, Tapias V, et al. Melatonin counteracts inducible mitochondrial nitric oxide synthase-dependent mitochondrial dysfunction in skeletal muscle of septic mice. *J Pineal Res*. 2006;40:71–78. doi:10.1111/j.1600-079X.2005.00281.x
25. Rodríguez MI, Carretero M, Escames G, et al. Chronic melatonin treatment prevents age-dependent cardiac mitochondrial dysfunction in senescence-accelerated mice. *Free Radic Res*. 2017;41:15–24. doi:10.1080/10715760600936359.
26. Rodríguez MI, Escames G, López LC, et al. Improved mitochondrial function and increased life span after chronic melatonin treatment in senescent prone mice. *Exp Gerontol*. 2008;43:749–756. doi:10.1016/j.exger.2008.04.003
27. Leonardo-Mendonça RC, Martinez-Nicolas A, de Teresa Galván C, et al. The benefits of four weeks of melatonin treatment on circadian patterns in resistance-trained athletes. *Chronobiol Int*. 2015;32:1125–1134. doi:10.3109/07420528.2015.1069830
28. Leonardo-Mendonça RC, Ocaña-Wilhelmi J, de Haro T, et al. The benefit of a supplement with the antioxidant melatonin on redox status and muscle damage in resistance-trained athletes. *Appl Physiol Nutr Metab*. 2017;42:700–707. doi:10.1139/apnm-2016-0677
29. Sayed RK, de Leonardis EC, Guerrero-Martínez JA, et al. Identification of morphological markers of sarcopenia at early stage of aging in skeletal muscle of mice. *Exp Gerontol*. 2016;83:22–30. doi:10.1016/j.exger.2016.07.007
30. Ebihara S, Marks T, Hudson DJ, Menaker M. Genetic control of melatonin synthesis in the pineal gland of the mouse. *Science*. 1986;231:491–493.
31. Roseboom PH, Namboodiri MA, Zimonjic DB, et al. Natural melatonin 'knockdown' in C57BL/6J mice: rare mechanism truncates serotonin N-acetyltransferase. *Brain Res Mol Brain Res*. 1998;63:189–197.
32. Khaldy H, León J, Escames G, Bikjdaouene L, García JJ, Acuña-Castroviejo D. Circadian rhythms of dopamine and dihydroxyphenyl acetic acid in the mouse striatum: effects of pinealectomy and of melatonin treatment. *Neuroendocrinology*. 2002;75:201–208. doi:10.1159/000048238
33. López A, Ortiz F, Doerrier C, et al. Mitochondrial impairment and melatonin protection in parkinsonian mice do not depend of inducible or neuronal nitric oxide synthases. *PLoS One*. 2017;12:e0183090. doi:10.1371/journal.pone.0183090
34. Whitehead JC, Hildebrand BA, Sun M, et al. A clinical frailty index in aging mice: comparisons with frailty index data in humans. *J Gerontol A Biol Sci Med Sci*. 2014;69:621–632. doi:10.1093/gerona/glt136
35. Liu H, Graber TG, Ferguson-Stegall L, Thompson LV. Clinically relevant frailty index for mice. *J Gerontol A Biol Sci Med Sci*. 2014;69:1485–1491. doi:10.1093/gerona/glt188
36. Feridooni HA, Sun MH, Rockwood K, Howlett SE. Reliability of a frailty index based on the clinical assessment of health deficits in male C57BL/6J mice. *J Gerontol A Biol Sci Med Sci*. 2015;70:686–693. doi:10.1093/gerona/glu161
37. Yamada Y, Kemniz JW, Weindruch R, et al. Caloric restriction and healthy life span: frail phenotype of nonhuman primates in the Wisconsin national primate research center caloric restriction study. *J Gerontol A Biol Sci Med Sci*. 2017;73:273–278. doi:10.1093/gerona/glx059
38. Kane AE, Hilmer SN, Boyer D, et al. Impact of longevity interventions on a validated mouse clinical frailty index. *J Gerontol A Biol Sci Med Sci*. 2016;71:333–339. doi:10.1093/gerona/glu315
39. Gomez-Cabrera MC, Garcia-Valles R, Rodriguez-Mañas L, et al. A new frailty score for experimental animals based on the clinical phenotype: inactivity as a model of frailty. *J Gerontol A Biol Sci Med Sci*. 2017;72:885–891. doi:10.1093/gerona/glw337
40. Parks RJ, Fares E, Macdonald JK, et al. A procedure for creating a frailty index based on deficit accumulation in aging mice. *J Gerontol A Biol Sci Med Sci*. 2012;67:217–227. doi:10.1093/gerona/glr193

41. Harris HF. On the rapid conversion of haematoxylin into haematin in staining reactions. *J Appl Microsc Lab Methods*. 1900;3:777.
42. Curtis F. Méthode de colorationélective du tissueconjonctif. *C. R. Soc. Biol*. 1905;58:1038–1040.
43. Crossmon G. A modification of Mallory's connective tissue stain with a discussion of the principles involved. *Anat Rec*. 1937;69:33–38. doi:10.1002/ar.1090690105
44. Latt SA, Stetten G, Juergens LA, Willard HF, Scher CD. Recent developments in the detection of deoxyribonucleic acid synthesis by 33258 Hoechst fluorescence. *J Histochem Cytochem*. 1975;23:493–505.
45. Reynolds ES. The use of lead citrate at high pH as an electron-opaque stain in electron microscopy. *J Cell Biol*. 1963;17:208–212.
46. Figueiredo PA, Ferreira RM, Appell HJ, Duarte JA. Age-induced morphological, biochemical, and functional alterations in isolated mitochondria from murine skeletal muscle. *J Gerontol A Biol Sci Med Sci*. 2008;63:350–359.
47. Roubenoff R, Hunghes VA. Sarcopenia: current concepts. *J Gerontol A Biol Sci Med Sci*. 2000;55:M716–M724.
48. Lang T, Streeper T, Cawthon P, Baldwin K, Taaffe DR, Harris TB. Sarcopenia: etiology, clinical consequences, intervention, and assessment. *Osteoporos Int*. 2010;21:543–559. doi:10.1007/s00198-009-1059-y
49. Gladden LB. Muscle as a consumer of lactate. *Med Sci Sports Exerc*. 2000;32:764–771.
50. Masuda S, Hayashi T, Egawa T, Taguchi S. Evidence for differential regulation of lactate metabolic properties in aged and unloaded rat skeletal muscle. *Exp Gerontol*. 2009;44:280–288. doi:10.1016/j.exger.2008.12.003
51. Romanick MA, Rakoczy SG, Brown-Borg HM. Long-lived Ames dwarf mouse exhibits increased antioxidant defense in skeletal muscle. *Mech Ageing Dev*. 2004;125:269–281. doi:10.1016/j.mad.2004.02.001
52. Mitchell WK, Williams J, Atherton P, Larvin M, Lund J, Narici M. Sarcopenia, dynapenia, and the impact of advancing age on human skeletal muscle size and strength; a quantitative review. *Front Physiol*. 2012;3:260. doi:10.3389/fphys.2012.00260
53. Visser M, Goodpaster BH, Kritchevsky SB, et al. Muscle mass, muscle strength, and muscle fat infiltration as predictors of incident mobility limitations in well-functioning older persons. *J Gerontol A Biol Sci Med Sci*. 2005;60:324–333.
54. Newman AB, Kupelian V, Visser M, et al. Strength, but not muscle mass, is associated with mortality in the health, aging and body composition study cohort. *J Gerontol A Biol Sci Med Sci*. 2006;61:72–77.
55. Listrat A, Lebret B, Louveau I, et al. How muscle structure and composition influence meat and flesh quality. *Sci World J*. 2016;2016:3182746. doi:10.1155/2016/3182746
56. Kovanen V, Suominen H, Risteli J, Risteli L. Type IV collagen and laminin in slow and fast skeletal muscle in rats – effects of age and life-time endurance training. *Coll Relat Res*. 1988;8:145–153.
57. Zhang C, Gao Y. Effects of aging on the lateral transmission of force in rat skeletal muscle. *J Biomech*. 2014;47:944–948. PMID:24507947.
58. Yamada Y, Yoshida T, Yokoyama K, et al. The extracelular to intracellular water ratio in upper legs is negatively associated with skeletal muscle strength and gait speed in older people. *J Gerontol A Biol Sci Med Sci*. 2017;72:293–298.
59. Narita S, Yorifuji H. Centrally nucleated fibers (CNFs) compensate the fragility of myofibers in mdx mouse. *Neuroreport*. 1999;10:3233–3235.
60. Marzetti E, Calvani R, Cesari M, et al. Mitochondrial dysfunction and sarcopenia of aging: from signaling pathways to clinical trials. *Int J Biochem Cell Biol*. 2013;45:2288–2301. doi:10.1016/j.biocel.2013.06.024
61. Shigenaga MK, Hagen TM, Ames BN. Oxidative damage and mitochondrial decay in aging. *Proc Natl Acad Sci USA*. 1994;91:10771–10778.
62. Salminen A, Kaarniranta K, Kauppinen A. Inflammaging: disturbed interplay between autophagy and inflammasomes. *Aging*. 2012;4:166–175. doi:10.18632/aging.100444
63. Quadrilatero J, Alway SE, Dupont-Versteegden EE. Skeletal muscle apoptotic response to physical activity: potential mechanisms for protection. *Appl Physiol Nutr Metab*. 2011;36:608–617. doi:10.1139/h11-064
64. Chevessier F, Marty I, Paturneau-Jouas M, Hantaï D, Verdière-Sahuqué M. Tubular aggregates are from whole sarcoplasmic reticulum origin: alterations in calcium binding protein expression in mouse skeletal muscle during aging. *Neuromuscul Disord*. 2004;14:208–216. doi:10.1016/j.nmd.2003.11.007
65. Agbulut O, Destombes J, Thiesson D, Butler-Browne G. Age-related appearance of tubular aggregates in the skeletal muscle of almost all male inbred mice. *Histochem Cell Biol*. 2000;114:477–481.
66. Schiaffino S. Tubular aggregates in skeletal muscle: just a special type of protein aggregates? *Neuromuscul Disord*. 2012;22:199–207. doi:10.1016/j.nmd.2011.10.005
67. Novotová M, Zahradník I, Brochier G, Pavlovicová M, Bigard X, Ventura-Clapier R. Joint participation of mitochondria and sarcoplasmic reticulum in the formation of tubular aggregates in gastrocnemius muscle of $CK^{-/-}$ mice. *Eur J Cell Biol*. 2002;81:101–106. doi:10.1078/0171-9335-00230
68. Acuna-Castroviejo D, Escames G, Rodriguez MI, Lopez LC. Melatonin role in the mitochondrial function. *Front Biosci*. 2007;12:947–963.
69. Escames G, Ozturk G, Baño-Otálora B, et al. Exercise and melatonin in humans: reciprocal benefits. *J Pineal Res*. 2012;52:1–11. doi:10.1111/j.1600-079X.2011.00924.x
70. Venegas C, García JA, Escames G, et al. Extrapineal melatonin: analysis of its subcellular distribution and daily fluctuations. *J Pineal Res*. 2012;52:217–227. doi:10.1111/j.1600-079X.2011.00931.x
71. Teodoro BG, Baraldi FG, Sampaio I. Melatonin prevents mitochondrial dysfunction and insulin resistance in rat skeletal muscle. *J Pineal Res*. 2014;57:155–167.
72. Galley HF, Lowes DA, Allen L, Cameron G, Aucott LS, Webster NR. Melatonin as a potential therapy for sepsis: a phase I dose escalation study and an ex vivo whole blood model under conditions of sepsis. *J Pineal Res*. 2014;56:427–438. doi:10.1111/jpi.12134
73. Weishaupt JH, Bartels C, Pölking E, et al. Reduced oxidative damage in ALS by high-dose enteral melatonin treatment. *J Pineal Res*. 2006;41:313–323. doi:10.1111/j.1600-079X.2006.00377.x
74. Coto-Montes A, Boga JA, Tan DX, Reiter RJ. Melatonin as a potential agent in the treatment of sarcopenia. *Int J Mol Sci*. 2016;1771. doi:10.3390/ijms17101771
75. Teodoro BG, Baraldi FG, Sampaio IH, et al. Melatonin prevents mitochondrial dysfunction and insulin resistance in rat skeletal muscle. *J Pineal Res*. 2014;57:155–167. doi:10.1111/jpi.12157